UNIVERSITY OF OKLAHOMA

GRADUATE COLLEGE

DFT-Derived Location and Hydroxide Coordination of Lanthanum Ions in Zeolite Y Structures

A THESIS SUBMITTED TO THE GRADUATE FACULTY

in partial fulfillment of the requirements for the Degree of

MASTER OF SCIENCE

By

Jacob P. Crouch

Norman, Oklahoma

2021

DFT-Derived Location and Hydroxide Coordination of Lanthanum Ions in Zeolite Y Structures

A THESIS APPROVED FOR THE

SCHOOL OF CHEMICAL, BIOLOGICAL AND MATERIALS ENGINEERING

BY THE COMMITTEE CONSISTING OF

Dr. Bin Wang, Chair

Dr. Daniel Resasco

Dr. Lance Lobban

Acknowledgements

This work was supported by the U.S. Department of Energy, Office of Science, Basic Energy Sciences under Award Number DE-SC0018284. The computational research used supercomputer resource of OU Supercomputing Center for Education & Research (OSCER) at the University of Oklahoma and the National Energy Research Scientific Computing Center (NERSC), a U.S. Department of Energy Office of Science User Facility.

I would like to thank my advisor and committee chair Dr. Wang for agreeing to chair this committee and for instructing me on how to carry out DFT calculations using VASP. His insightful comments and patience addressing my questions and concerns, have inspired me to delve into the details of research publications and ponder the scientific principles responsible for the results, both from literature and my own computational experiments.

I am grateful to all the wonderful people in Dr. Wang's research group, Computational Materials and Chemistry (cmc) Group, especially Yu Yan who guided me through the process of operating the supercomputer interface and taught me how to submit batch jobs online and convert molecular position files into the POSCAR format.

I would also like to thank Dr. Resasco, Dr. Lobban, for agreeing to join in the committee. Their insightful comments throughout my time working on this project have been invaluable, allowing me to better present and analyze the finding of my research.

Table of Contents

Abstract

Fluid Catalytic Cracking is a process of great interest in oil refining. This process is governed by the stability and activity of acid sites held within zeolite frameworks. Rare earth exchanged, specifically lanthanum exchanged, zeolite Y is known to have increased resistance to framework dealumination. This study examines lanthanum exchanged zeolite Y (Si/Al = 3) through the use of density functional theory calculations with the purpose of elucidating the location and nature of La species held within the zeolite framework. This is accomplished through calculation of silicon chemical shifts to determine the arrangement of Al atoms in the framework. Followed by stability calculations for the position and hydroxide coordination of $La(OH)_X$ (X is the number of OH groups and ranges from 0 to 2) species at each of the seven unique ion exchange position in zeolite Y. The most stable single La position is found to be at the center of the hexagonal prism (site I) as a bare La^{3+} cation, followed closely by LaOH located atop the hexagonal prism (site I'). Lanthanum clusters of three are not preferred. However, La clusters of two inside the sodalite cage are preferred over all other lanthanum orientations. After finding the most stable positions, proton chemical shifts were calculated for lanthanum containing structures and compared to corresponding deprotonation energies, however, no trend between the two is found. Values of deprotonation energy for H connected to La molecules are too high to be strong Bronsted acid sites, though they could potentially act as strong Lewis acid sites.

Chapter 1: Introduction

1.1: Background of Petroleum Refining:

Fluid catalytic cracking (FCC) is a prominent process in the refining of petroleum oil into gasoline and other products such as light olefins. In 2014, nearly half of all refineries used the FCC process[1]. FCC is a process by which larger hydrocarbons (from petroleum) are broken down into smaller products such as octane, heptane, etc. This is accomplished using a riser reactor. This reactor has steam and catalyst particles fed concurrently with the oil stream. The catalyst becomes coked and is separated at the top of the reactor and is then sent to a regenerator which burns off the coke and sends the catalyst back to the riser reactor, and the process repeats. The products stream is separated into several different streams as shown in Figure 1[2].

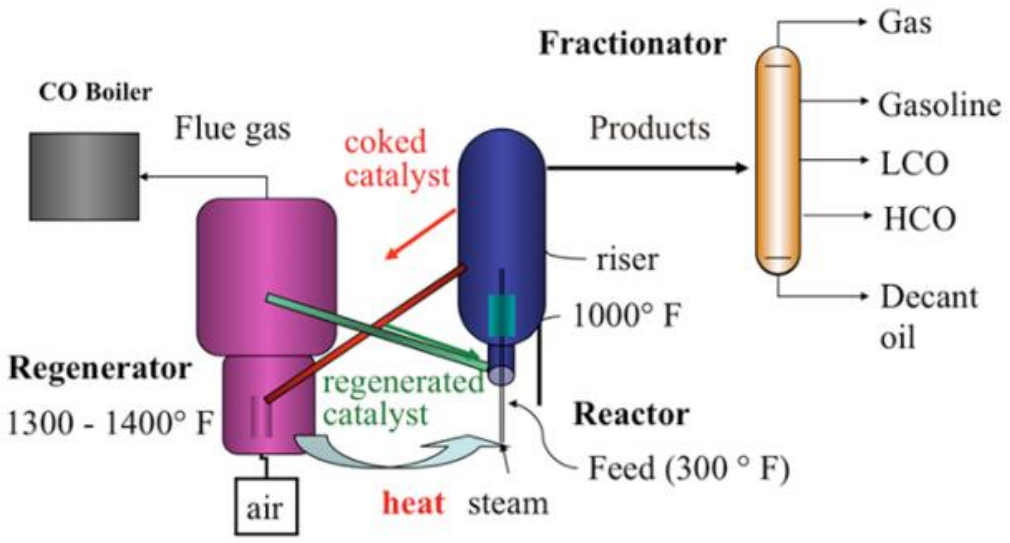

Figure 1: FCC process, courtesy of Penn State University College of Earth and Mineral Sciences[2].

Commercial production of petroleum was first introduced in 1859 in Pennsylvania. As the need for more gasoline increased, so did the need for a better refining process. Dr. Burton, at Standard Oil of Indiana was the first to utilize one such improvement. He introduced a high pressure and temperature process that allowed for the larger molecules to be broken down into more suitable species for use in engines. In following years, some additives were used to improve the process. In 1923, tetraethyl led was added to some of the refineries' processes, but this was not enough. An aluminum chloride catalyst was tested but was economically unrealistic[3]. Later in 1940, the first large scale plant using a silica-alumina catalyst started production in Paulsboro, New Jersey[4]. In the 1960s and 1970s, zeolite catalysts began their appearance in oil refining with the patent of Zeolite Y in 1964[5]. Today, Zeolite Y is used as the primary catalyst in FCC processes to produce gasoline-range molecules. Zeolites are microporous catalysts usually made of mostly silicon and oxygen (see Figure 2.).

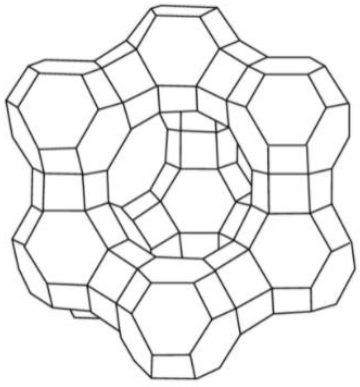

Figure 2. Representation of Zeolite Y. Each vertex represents a silicon atom and in between each Si there is an oxygen atom. The hole in the center is the supercage and the smaller cages are sodalite cages. (Image courtesy of Dr. F. Handan Tezel)[6].

Aluminum can replace the silicon to create an active site for molecular adsorption, while the pores can restrict larger molecules from certain active sites[7]. Zeolites have greatly improved selectivity and productivity of petroleum refining processes[8]. Selectivity helps to maintain control over byproducts reducing contaminants[9]. Along with these benefits, zeolites have some process design challenges. One issue with zeolite catalysts derives from the severe process conditions required for Fluid Catalytic Cracking. The high pressure and temperature (reaction around 538 °C and regeneration at 700 °C) causes structural collapse to eventually occurs[10]. The stability and ability to recover activity through regeneration (usually by burning coke) are the determining factors in the FCC process, so it is important to resist collapse. One well-known way to improve the resistance to structural damage and to retain activity is by introducing rare earth elements (e.g. lanthanum and cerium), thus obtaining rare earth exchanged zeolite Y (REY)[11].

1.2 REY: Stability

Rare earth exchanged zeolite Y (REY) has increased stability, as shown in the mid-1980s, when Li and Rees investigated the effects of temperature on faujasite structures and found that Lanthanum exchange increased the temperature required to collapse the framework[12]. Much research has been performed on rare earth exchanged zeolites and found that lanthanum exchanged zeolite Y (LaY) is of special interest[13, 14]. LaY is more active than zeolite HY and has greater stability[15]. During the 1980s, J. W. Roelofsenm and coworkers found that lanthanum within zeolite Y greatly inhibits dealumination of the framework

allowing for the preservation of active sites[16]. This in turn provides greater activity for the zeolite catalyst[17]. In order to better understand the increase in stability found in rare earth exchanged zeolite Y, it is important to understand the nature and location of lanthanum containing molecules within the zeolite framework. The location is influenced by the lanthanum loading, silicon aluminum ratio (Si/Al) and temperature, the location of the lanthanum cation could be inside the super cage, sodalite cage, or hexagonal prisms (sometimes referred to as sodalite bridges). La ions cannot enter the sodalite cages at low temperatures due to the small pore size. However, if the temperature is increased beyond 60 degrees Celsius (which is common in industrial processes), the lanthanum ions begin to diffuse into the sodalite cages and hexagonal prisms[18]. It is important to understand the position of La in the zeolite framework as this allows for improved understanding of the underlying principles governing the stability, activity, and selectivity caused by rare earth exchange[19]. This leads to improved process design in oil refineries. The location of the lanthanum ion is strongly influenced by the location of surrounding Al sites. Louwen, and coworkers found that the aluminum contained in the zeolite framework (Si/Al = 3) does not exist in the most stable configuration by comparing NMR calculations to experimental results[20]. They proceeded to determine the most stable position for a La^{3+} ion within zeolite Y, in the presence and absence of water based on energetics calculations, and found that the cation was located at the I position which is inside the sodalite bridge[10]. In 2011, Sch€ußler and coworkers examined the increased stability from lanthanum clusters held within the sodalite and

noticed additional stability for La cations in the supercage due to coordination with $(OH)^-$ groups in the clusters[21]. Scherzer et al found that the unit cell size (based on XRD) decreases and framework vibrations shift towards higher frequencies proportionally to increased harshness of the thermal treatment. This result is associated with structural collapse. They find that this effect has a linear relationship with the amount of rare earth in the framework[22]. Supporting this, Rees, et al found that the temperature required to collapse the framework found using differential thermal analysis moves to higher temperatures when there is rare earth exchange[12].

1.3 REY: Infrared Spectroscopy

Much research was performed on REY utilizing IR-analysis[23-25]. IR analysis is a process by which infrared light's interactions with molecules is measured. The absorption, emission and reflection provide insight into the adsorption of molecules and the species present in a sample[26, 27]. In the case of LaY, this can help us to better understand the nature and location of lanthanum present in the zeolite framework as well as inform us of structural changes caused by thermal treatment. IR vibrational peaks for zeolite Y were assigned in 1971 by Flanigen et al.[28]. In 1986, Roelofsen et al. explain that the intensity of the stretch vibration peak around 790 cm^{-1} corresponds with the silicon aluminum ratio (SAR) and linearly with Al/(Al + Si) ratio. This peak is ideal for determining the silicon aluminum ratio as it is less effected than other peaks by water concentration, types of cations contained in the framework, and cation type and content[29]. The intensity of the IR peak found around 3747 cm^{-1} corresponds to

SiOH groups of amorphous silica alumina, the peak at 3743 cm^{-1} is assigned as terminal silanol groups associated with silica-aluminas rich in silicon, and the intensity of the 3730 cm^{-1} peak is found to correspond with terminal silanol groups on the crystal structure[17, 30]. The peak around 3680 cm^{-1} is found to correspond with aluminum hydroxide species[31, 32]. The bands around 3510 cm^{-1} is attributed to OH groups associated with rare earth species (3530 cm^{-1} is associated with lanthanum hydroxide groups). It is found that as the ionic radius of the exchanged rare earth increases this band becomes narrower and sharper. This effect is attributed as there only being one type of OH group associated with the rare earth cations[17]. This group is the focus of this study and La species examined are La^{3+}, $(LaOH)^{2+}$, $(La(OH)_2)^{1+}$, and clusters of $La(OH)_X$ groups. Other potential structures (e.g. La_2O_3) are not analyzed here.

1.4 REY: Nuclear Magnetic Resonance

Another useful characterization technique that is commonly employed is MAS NMR (Magic angle spinning nuclear magnetic resonance)[33-36]. NMR was first described in 1938 by I. I. Rabi et al. This technique disrupts nuclei in a strong magnetic field through the application of a weaker oscillating magnetic field, and the nuclei then respond by changing the population of spin-up and spin-down energy states and then sending out an electromagnetic signal. This signal is focused and then displayed[37]. This is possible since nuclei are electronically charged, and many have spin states and create a magnetic field. When an external magnetic field is applied, an oscillating weaker magnetic field responds near the nucleus. When this oscillating field has the same frequency as the nuclei's

magnetization, resonance occurs. The nuclei can gain energy and be excited to a higher energy state, the nuclei can then return to their original energy state which causes a signal emission matching the applied frequency. To ensure that the data is independent of the spectrometer used, a standard is used to compare the signal. The data is processed by taking the frequency of the sample, minus the frequency of the standard, all divided by the frequency of the spectrometer. This leaves a unitless measurement defined as parts per million or ppm, defined as the chemical shift. One aspect that affects chemical shifts the most is the shielding effect defined as the electron shell generating an opposite magnetic field as compared to the applied one, thus reducing the effect applied at the nuclei. Thus, a more electronegative nucleus will result in more shielding of the nucleus and thereby cause the chemical shift to increase (move toward lower fields). In addition, a local positive charge will generally cause the shielding to decrease and lower the chemical shift (move toward higher fields)[38, 39]. Unique peaks (x-axis chemical shift) depending on chemical species and environments then appear. The higher the intensity of the peak the more of that species is present (or there are overlapping peaks)[40-44]. NMR is a non-destructive technique, allowing for several analyses to be carried out on the same sample. Another advantage of NMR is that it does not require much sample preparation and is easily reproduced by experiments[45]. NMR provides insight into molecular environments allowing for better knowledge of which species are present in the sample and how much of the species exists[46, 47].

Bejoy Thomas et al used NMR on LaHY to reveal Al peaks at 56.14 and -0.54 ppm, these correspond with framework Al and octahedral Al respectively. Five major Silicon NMR peaks are found for tetrahedral Si. These peaks correspond with the number of Al species connected to the Si by one oxygen (Si – O – Al) and ranges from Si(0Al) to Si(4Al)[48]. This is in good agreement with similar results for Si NMR from Klinowski J. et al during the 1980s[20]. While NMR can help to determine the acid site locations, calculation of the deprotonation energy can provide insight into the relative strength of the acid sites.

1.5 REY: Deprotonation Energy

Deprotonation energy (DPE) is a measure of acid strength and specifies the energy required to remove a given proton[49, 50]. This is useful to obtain as it governs some reactions energy barriers based on proton location, however, the exact DPE of individual protons inside the zeolite framework can be difficult to obtain using physical experiments[51, 52]. However, computational experimentation (using Density Functional Theory) allows for the determination of the DPE for any proton provided that an accurate model of the system can be generated. In 2013, Na Wang et al, determined the DPE for a large variety of protons in the zeolite HY framework in the absence of rare earth using computational methods[50]. The deprotonation energy is important for comparison between computational values and experimental estimates. This comparison helps to determine the location and orientation of protons inside the structure as well as confirm the accuracy of the computational model of the structure[53-55].

1.6 REY: Atomistic Simulations

Density Functional Theory (DFT) is a useful computational technique used by many scientists that allows for experimentation on systems without physically running the experiments[10, 56-60]. This is especially useful when other characterization techniques cannot give a precise picture of what is happening inside of a system. This is the case with rare earth exchanged zeolite Y. To determine the exact location of lanthanum, computational data can be compared with experimental data, NMR being of special interest. When the two systems (real and computational) give similar results, the simulated system becomes representative of the physical samples. Density Functional Theory is a more recent development, having its origins date back to the 1900s, and even then it was not strongly implemented until after 1990 due to issues with accuracy and computational efficiency[61, 62]. In 1965, an early DFT model, titled after its creators, Kohn–Sham DFT was formulated[63]. The idea behind DFT programs is to approximate the Schrödinger[64, 65] and Dirac[66-68] equations using quantum mechanical theories. The computation is simplified and made possible by calculating properties as functionals of electron density[69, 70]. Some of the earliest density functional approximations were carried out by Fermi and Thomas, though they did not refer to it by this terminology[71, 72]. Practical applications of DFT computations were enhanced using the simplification of the Hartree–Fock[73, 74] method as proposed by Slater in 1951 in the publication "A Simplification of the Hartree-Fock Method"[75]. The addition of exchange-correlation energy gradients during the 1980s allowed for considerable improvement of computational

accuracy[76-78]. Accuracy was further enhanced by the calculation of the second derivatives of electron density. These advances in computational chemistry have a negligible effect on computational expense (time required to run a calculation) and a significant decrease in inaccuracy[79-81]. Density functional theory became even more accurate with the introduction of hybrid functionals. Hybrid functionals are approximations made using both the exact exchange from the Hartree-Fock Method[73, 74] and exchange correlation energy gradients[82-85]. Hybrid functionals were not without a downside. In exchange for greater accuracy, computational time was increased[86]. Today simulation packages that allow for DFT calculations of energy and chemical shifts have become more popular. One such simulation package is named VASP (Vienna Ab-initio Simulation Package). With its origins dating back to the late 1980s VASP can run energetics (or stability calculations) calculations which find the lowest energy for the structure. It can also run NMR and IR simulations providing the chemical shift and quadrupolar moments[87]. VASP is used by many researchers and is considered to be an accurate DFT simulation package[88-93]. VASP is utilized in this study to examine lanthanum exchanged zeolite Y.

1.7: Research Goals

Previous studies have provided insight into the properties of rare earth exchanged zeolite Y but have not yet provided a detailed account regarding the exact location and hydroxide coordination of lanthanum cations. The protons connected directly to oxygen atoms bonded with La species are of particular importance for increasing structural stability and potentially increasing the

number of active sites available in zeolite Y. In this work, we applied DFT calculations to determine the most stable position and number of hydroxide groups bonded with the lanthanum ion, using VASP for all calculations whilst considering Van der Waals interactions. Lanthanum clusters are included in the discussion and their stability is compared with that of single lanthanum ions. The deprotonation energy and proton chemical shifts are found and compared; however, no clear correlation was found between the two.

Chapter 2: Computational Methods

Computations for this DFT study were performed using the PBE (Perdew, Burke, Ernzerhof) functional on zeolite Y utilizing VASP[94]. Van der Waals interactions were included using the DFT-D3 method. Unit cells were optimized, allowing them to change, to account for unit cell expansion caused by the addition of La species[59, 90, 95]. A SAR (Silicon Aluminum Ratio) of 3 is used for this study as this is a common ratio in experiments and industry[10, 96]. Calculations involving thermodynamic stability were performed considering an energy difference of 10^{-6} eV to be converged. The KPOINTS was set to 3x3x3 to sample the Brillouin zone.

2.1 Aluminum Positions: Stability Calculations

In a study by Louwen and coworkers[10], a rhombohedral primitive cell was used to represent a quarter of the cubic unit cell of zeolite Y due to the face-centered symmetry. We adopted the initial form from this study and then further relaxed the structure using the aforementioned settings. Optimization of Zeolite

Y (SAR = 3) to determine the lowest energy state were first performed to determine the most probable and most stable structure. The rhombohedral cell consisted of 48 T sites of which 12 were occupied by Al atoms. Stability calculations were carried out for three structures, 3333, 4332, and 6600 with the unit cell size being optimized for minimum energy as well. The sequence of numbers 3333, 4332, or 6600 refers to the number of aluminum atoms contained in each sodalite bridge. Each bridge is made up of two of the following six membered rings (ignoring oxygen atoms) see Figure 3.

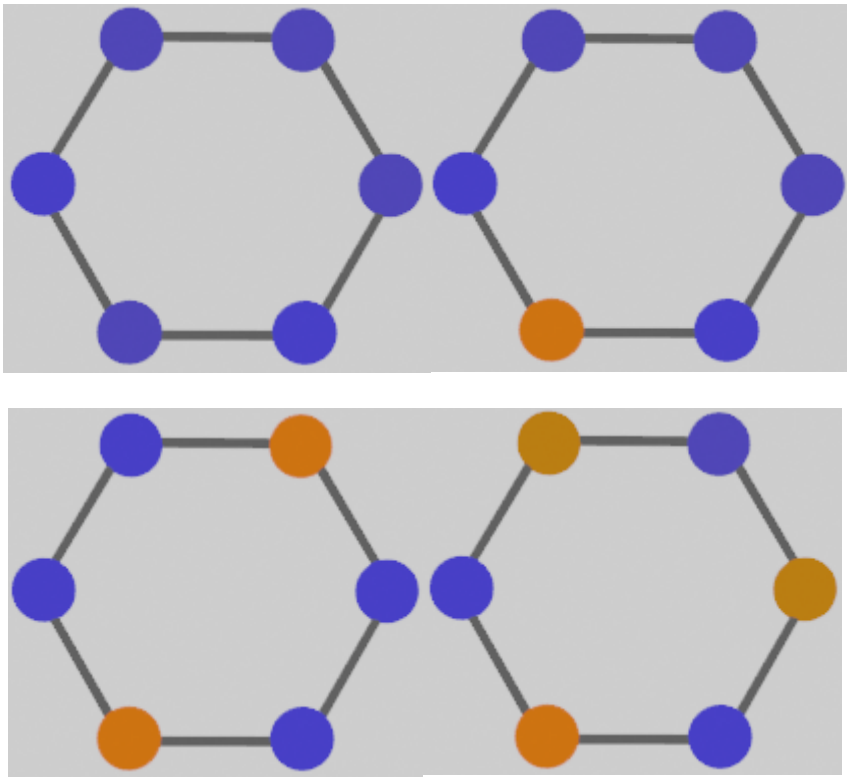

Figure 3. Aluminum distributions in six-membered ring environments. Orange and blue atoms represent Al and Si respectively. Oxygen atoms are not shown, simplifying the figure.

The Loewenstein's rule of avoiding Al-O-Al linkages was followed for placement of Al atoms[97]. Some violations to this rule have been recorded; however, these

orderings only occur in theoretical and very special cases[98-100]. Figure 4. shows the positions of sites within the framework (Figure 4.a) and the unit cell used for this study (Figure 4.b).

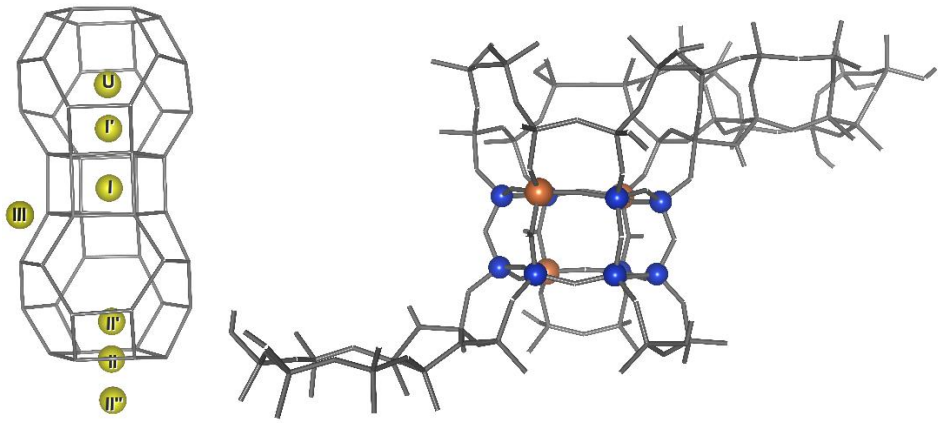

Figure 4. a) Representation of the unique ion exchange positions found in zeolite Y. These are the proposed locations of La in zeolite Y structures.

b) Unit cell of zeolite Y (4332) used for calculations with emphasis on the clearest sodalite bridge. Blue atoms are Si and orange are Al. Oxygen atoms are omitted for simplification of the figure.

2.2 Aluminum Positions: NMR

Chemical shift calculations were run using the linear response method[101, 102]. The linear response method, also referred to as density functional perturbation theory (DFPT), applies a perturbation to the system. In this study the perturbation is a magnetic field used to simulate the conditions experienced during experimental NMR. The chemical shift is then calculated allowing for comparison with results from physical samples[103]. For direct comparison the number of Al atoms adjacent to each Si atom were counted thus generating five

groups or NMR peaks (0 – 4 nearby Al). The average Si chemical shift was calculated for each of these groups and then plotted using a gaussian distribution. The graphs were used to compare the structures to previous studies[20, 48, 104] and the 4332 structure was selected, as this was the most similar to results from physical studies, and thus was used for the remainder of the calculations to save on computational expense. Chemical shifts were referenced to methane (for hydrogen), and tetramethyl-silane (for silicon).

2.3: Lanthanum

Next $La(OH)_x$ (x ranged between 0 and 2) was tested at each of the seven unique ion exchange positions within zeolite Y. For each position $La(OH)_x$ was placed into the structure and a corresponding quantity of protons removed from nearby aluminum sites to balance the charge. For $La(OH)_2$, one proton was removed, while for La three protons from nearby Al sites were removed. These structures were optimized, and their energies compared using the following formula where x is the number of hydroxide groups bonded with La.

$$E_R = E_{La} - E_Y - E_{La(OH)_3} + (3 - x)E_w$$

Where E_R is the relative energy used for comparison between structures.

E_{La} is the energy of the optimized structure including lanthanum,

E_Y is the energy of the 4332 structure before La-exchange,

E_{LaOH3} is the energy of $La(OH)_3$ in a vacuum, and

E_w is the energy of a water molecule in a vacuum.

Following this, clusters of two and three La cations, $La_2(OH)_3$ and $La_3O_5H_4$ respectively, were optimized both inside the sodalite cage and within the supercage. The relative energy of clusters is divided by the number of La ions so that a comparison may be accomplished. NMR calculations were performed for all these structures (sites I – U and cluster models) and chemical shifts obtained by referencing proton shifts to methane in a vacuum. A shift towards higher fields (more negative chemical shift) was expected for Silicon atoms nearby charge balancing aluminum sites. This is because with the removal of the nearby proton the positive charges are further away from the silicon nucleus thus resulting in more shielding which causes the chemical shift to move towards lower values. The proton chemical shift for framework hydrogen nearby the lanthanum cation was expected to increase since the addition of the nearby positive charge will result in less shielding by the electrons thereby causing a higher chemical shift to be observed. The deprotonation energy (DPE) was also calculated for protons connected with lanthanum cations for the most stable structures at each of the ion-exchange positions as well as for the lanthanum clusters. This was done by removing the proton in question and reoptimizing the structure. The value was obtained using the following formula.

$$DPE = E_{La} + E_{H+} - E_{-La}$$

E_{La} is the energy of the optimized structure including lanthanum as above,

E_{H+} is half of the energy of a H_2 molecule (energy of a hydrogen atom), and

E_{-La} is the energy of the reoptimized structure with a proton removed.

Chapter 3: Results and Discussion

3.1: Zeolite HY Stability

Aluminum positions were directly compared with one another as shown in Table 1. The relative energy shows that the 3333 structure is the most thermodynamically stable, followed closely by 4332 and then by 6600. The unit cell size for the 3333 structure is 24.834 Å. Our calculated value is similar to an experimental value of 24.6 Å which was also measured with a SAR equal to three. In order to be certain, we calculated the total energy once more using the hybrid functional, this reduces error caused by charge delocalization, and find the trend endures. A previous DFT study found that the 6600 structure was the most stable followed by 4332 and then by 3333, which is the reverse order from this study[10]. We believe this difference to be the result of the detailed computational methods, and think that the structure with an even distribution of Al, the 3333 structure, should be the most stable of the three as a result of containing more delocalized charges, while the Al clumping of the 6600 structure leads to energy penalties for the charge localization[105].

Table 1. Relative energies with respect to the most stable structure and optimized unit cell sizes (Angstroms) for each arrangement of aluminum atoms.

Distribution of 12 Al	**Relative Energy (kcal/mol)**	**Unit Cell Size**
Zeolite Y 6600	33.52	23.817
Zeolite Y 3333	0	24.834
Zeolite Y 4332	5.50	24.836

Though the 3333 arrangement is the most thermodynamically stable, this does not necessarily mean that it is the arrangement that occurs. Formation of the zeolite Y structure is not driven by only thermodynamic stability, but also by kinetic growth. The formation of the zeolite HY structure could cause Al atoms to be placed in a different arrangement if the kinetics of the process overcome the thermodynamic tendency towards minimum energy[106-108]. In order to determine the most realistic organization, chemical shift calculations for silicon are compared to results from NMR carried out on physical samples of zeolite HY.

3.2: Zeolite HY NMR

NMR spectra obtained for zeolite Y are shown in Figure 5. Reading the peaks from right to left, the first peak is for Si with four Al neighbors (only seen in 6600), the second is associated with three Al neighbors, the third with two, the fourth peak is for one Al neighbor, and the last peak is for silicon atoms with no Al neighbors[48].

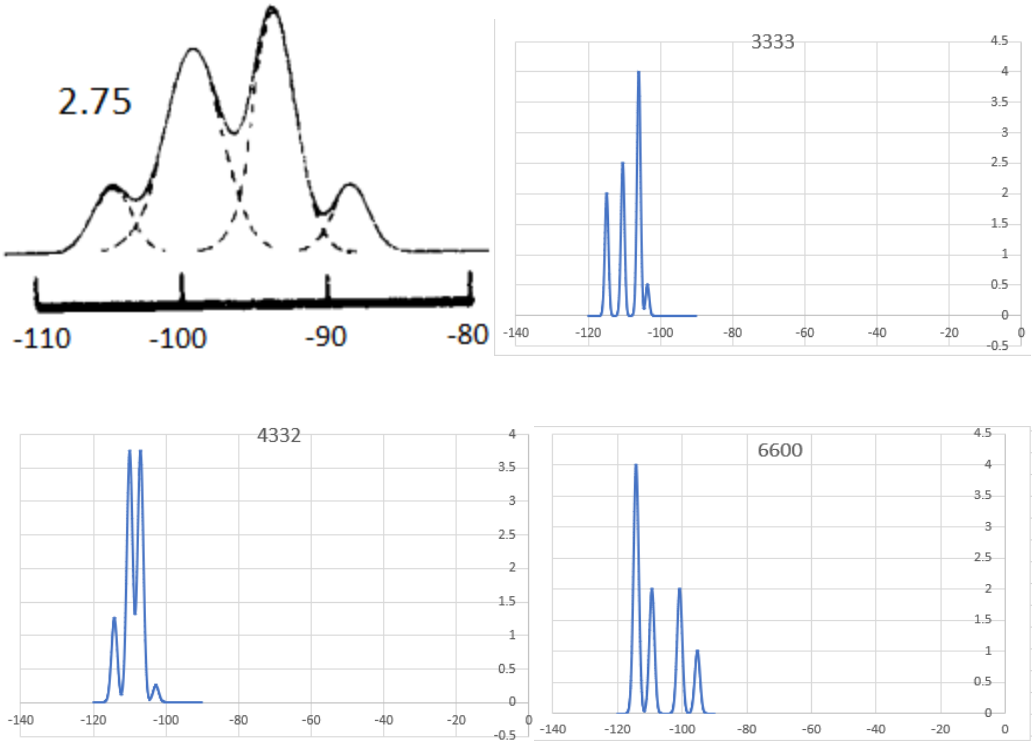

Figure 5. NMR Spectra. The first is a result from Klinowski's 1982 publication[20]. The other three spectrum were generated using a gaussian distribution of the results from this study.

Upon comparation of the three HY NMR spectra with the results from Klinowski[20], Pablo García[109], and Melchior[104], we find that the 4332 structure best matches the experimental NMR data (Figure 5). Therefore, the 4332 structure is used for the lanthanum calculations as this is the most realistic arrangement of aluminum atoms. This agrees with Louwen's conclusion for the most likely organization of Al atoms[10]. The most likely organization is not the only arrangment that will occur in a real sample, but it is the most common. It is worth noting that the 4332 structure is only slightly less stable than the 3333 structure. The non-uniform placement of Al resulting in the 4332 structure is likely the result of the complex processes that occur during the synthesis of zeolite Y causing thermodynamic equilibrium to never be fully reached. The sodalite

bridges contained in the 4332 structure can be seen using Figure 6 as it can be difficult to distinguish sodalite bridges from the unit cell.

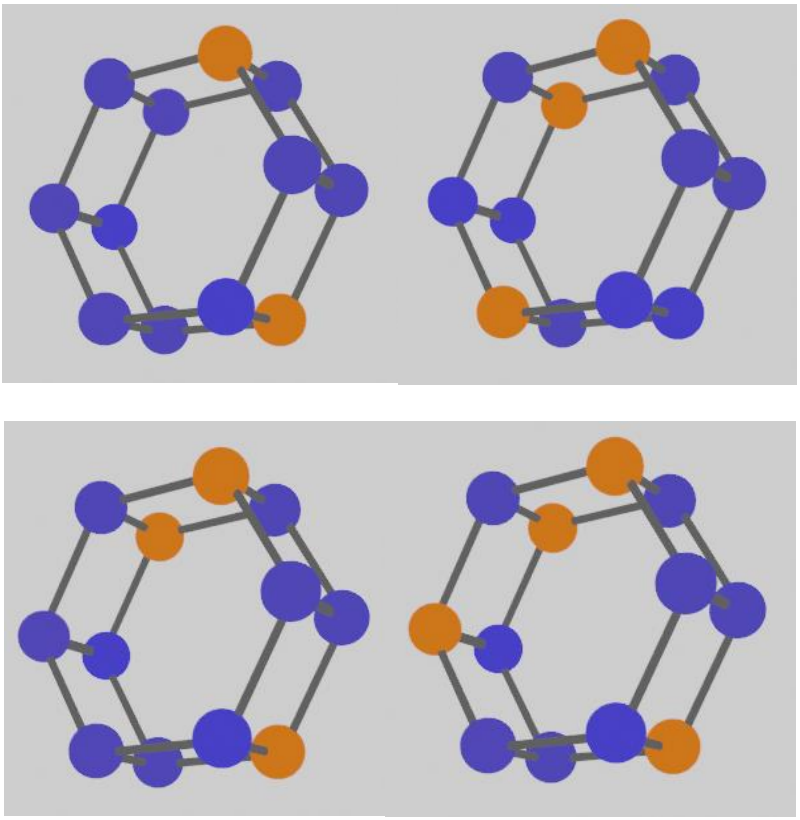

Figure 6. The four sodalite bridges that construct the 4332 zeolite Y environment. Orange and blue atoms represent Al and Si atoms respectively. Oxygen atoms are omitted. Note that the rings with three Al atoms are identical, just oriented differently for emphasis.

3.3: Zeolite LaY Stability

Proceeding with the 4332 arrangement of Al to represent zeolite Y with a SAR of three, the calculations are continued by positioning lanthanum in each of the seven unique sites shown in Figure 4. Table 2 compares the stability of each site to one another. According to computations, low amounts of bare La^{3+} should show preference to site I, located in the center of the sodalite bridge, which is

consistent with findings from Louwen and coworkers for La^{3+} without water coordination [10]. For site I, the three positive charges of La are stabilized by the negative charges of Al species in the framework on the sodalite bridge. The next most stable single La structure is LaOH at the I' position, located just above the sodalite bridge going into the sodalite cage. The positive charges are balanced by one OH group attached to La and by negative charges induced by two Al sites. The stability at site II is very low. Lanthanum with only one OH group cannot exist at site II (in the hexagonal window between the sodalite cage and supercage). This is due to the direction of the OH group forcing the LaOH to move to either II' or II''. The only form of the $La(OH)_X$ that could occupy this site was $La(OH)_2$ since it could point OH groups in opposite directions, (one facing into the sodalite cage and the other into the supercage) which is an unfavorable orientation.

Table 2. Relative energies comparing the most stable configuration at each site, including clusters both inside and outside the sodalite. The energy of the clusters is divided by the lanthanum count.

Site	Type	Relative Energy (eV)
I	La	-3.36
I′	LaOH	-3.22
II	$La(OH)_2$	-1.58
II′	LaOH	-2.42
II″	LaOH	-2.95
III	$La(OH)_2$	-2.86
U	LaOH	-2.28
Sodalite	Two Cluster	-3.39
Sodalite	Three Cluster	-2.09
Super Cage	Two Cluster	-2.87
Super Cage	Three Cluster	-2.38

Clustering with two La in the sodalite cage is preferred over distribution over two sites. The value per La is -3.39 eV and is more stable than -3.36 eV for isolated La^{3+} at site I located in the middle of the sodalite bridge (sometimes referred to as hexagonal prism). Increasing to a cluster of three La species, produces a formation energy of -2.09 eV. The stability is reduced. This is likely the result of limited space inside the sodalite cage. This forces the large cluster to be closer to the walls, causing a decrease in stability. However, clustering with three La in the sodalite is preferred over site II. Clustering within the super cage should not

occur except when La is highly loaded, thus filling the most stable arrangements causing the clusters to be more stable. Clusters of three are generally not preferred due to their size and a general lack of Al sites available for charge balancing. LaOH is the most stable configuration at four of the seven unique sites due to their being plenty of Al sites to balance the charge. La^{3+} was less stable at most sites than LaOH or $La(OH)_2$ due to a lack of three nearby Al sites to even out the charge. However, at the I position, located in the center of the sodalite bridge, there are enough close by sites to balance the charge which resulted in increased stability. Included below are the 11 sites described in Table 2.

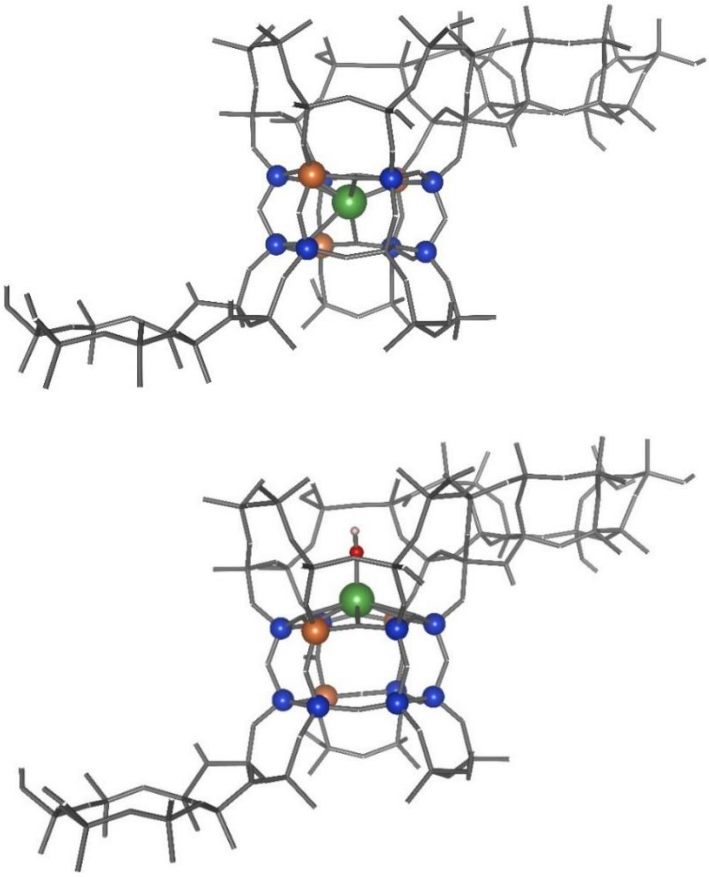

Figure 7. Most stable structures for ion exchange positions I and I' respectively.

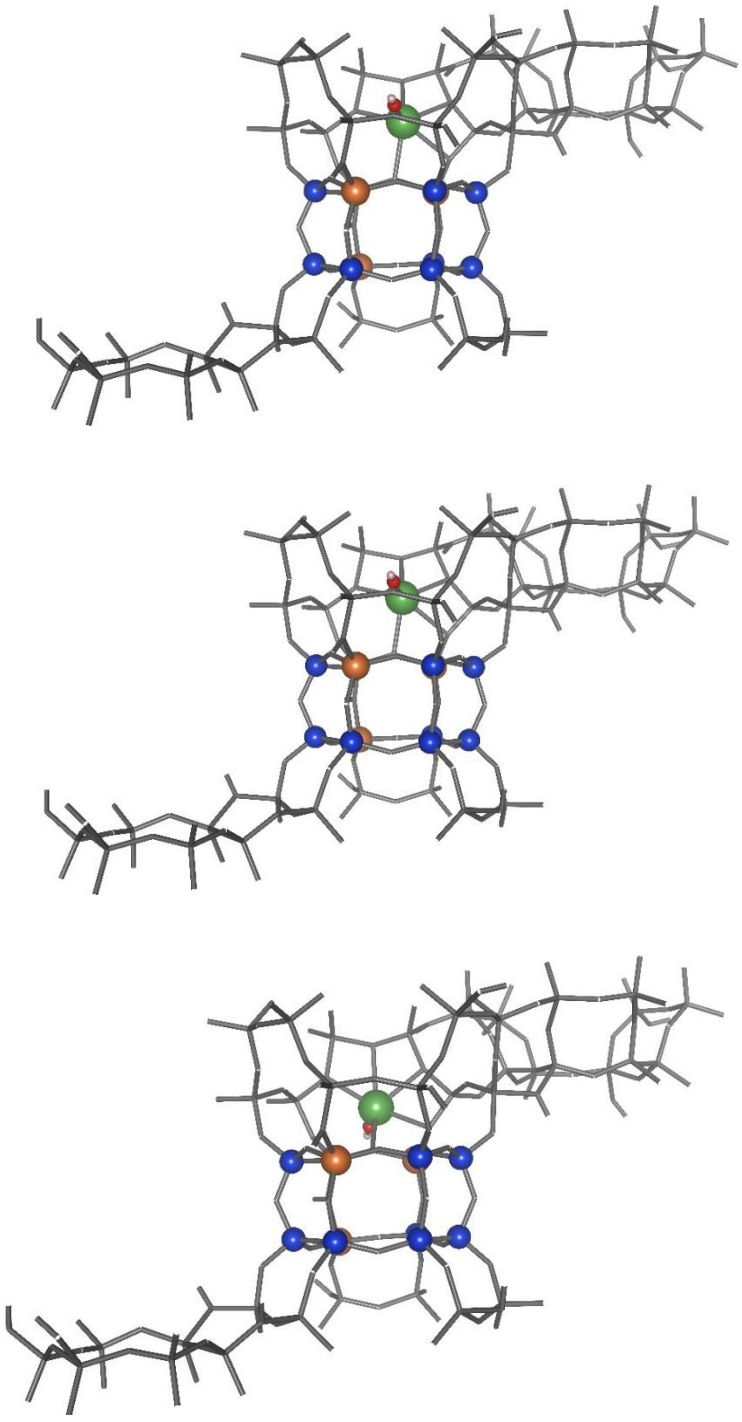

Figure 8. Most stable structures for ion exchange positions II, II', and II'' respectively. Note that on site II the second hydroxide group is present, it is merely hidden behind the La atom.

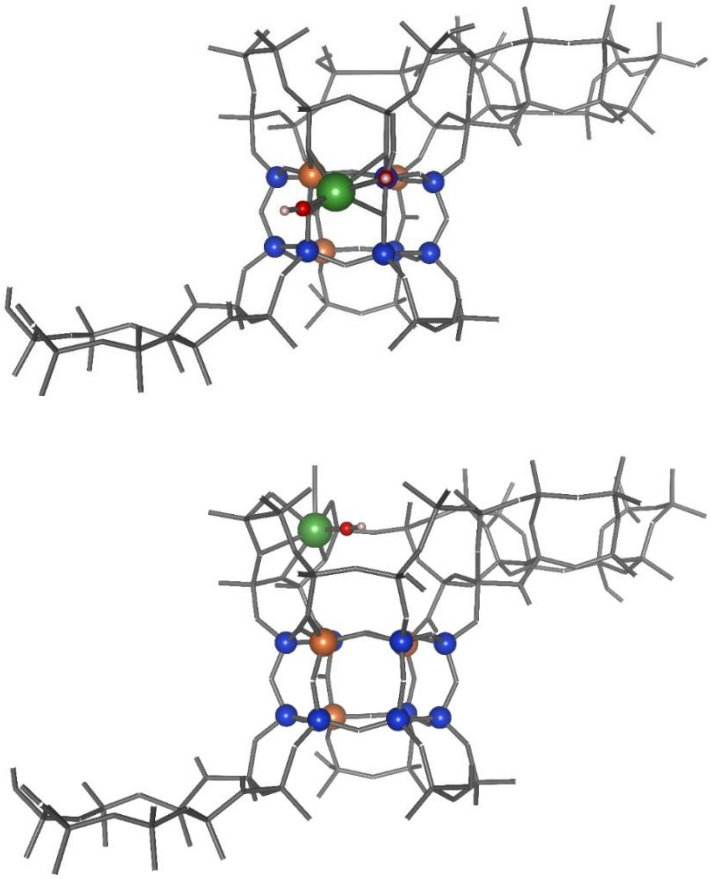

Figure 9. Most stable structures for ion exchange positions III and U respectively. U gravitates towards the walls of the sodalite cage for all hydroxide coordinations.

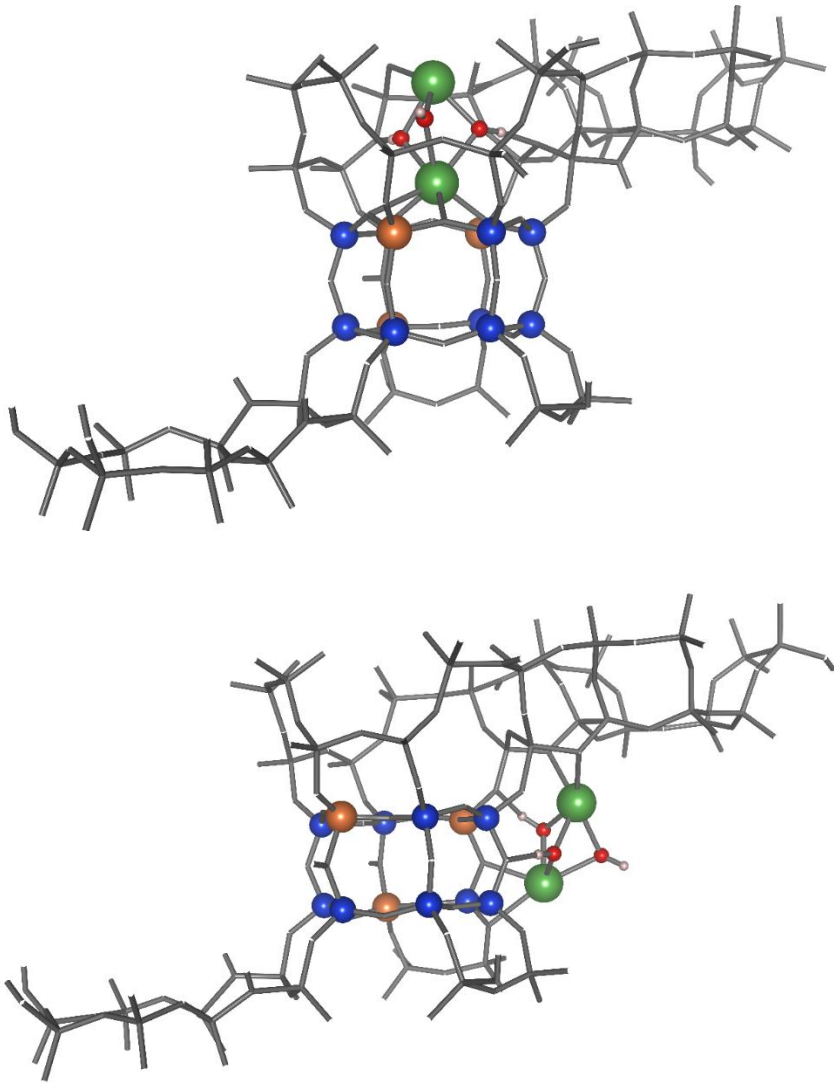

Figure 10. Most stable structures for La in clusters of two, both inside the sodalite cage and within the super cage.

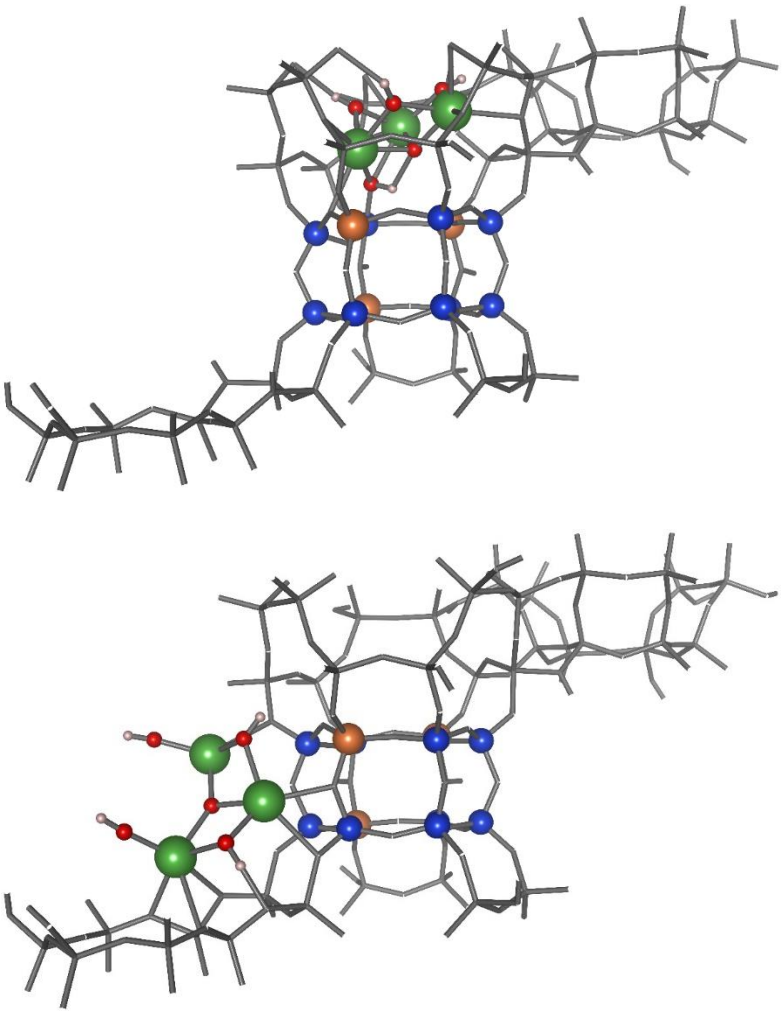

Figure 11. Most stable structures for La in clusters of three, both inside the sodalite cage and within the super cage.

3.4: Zeolite LaY NMR and DPE

Lanthanum species inside the zeolite pores, introduces new proton species. Without La, proton chemical shifts at the Bronsted acid sites are found between 3.3 and 4.0 ppm as shown in Figure 12.

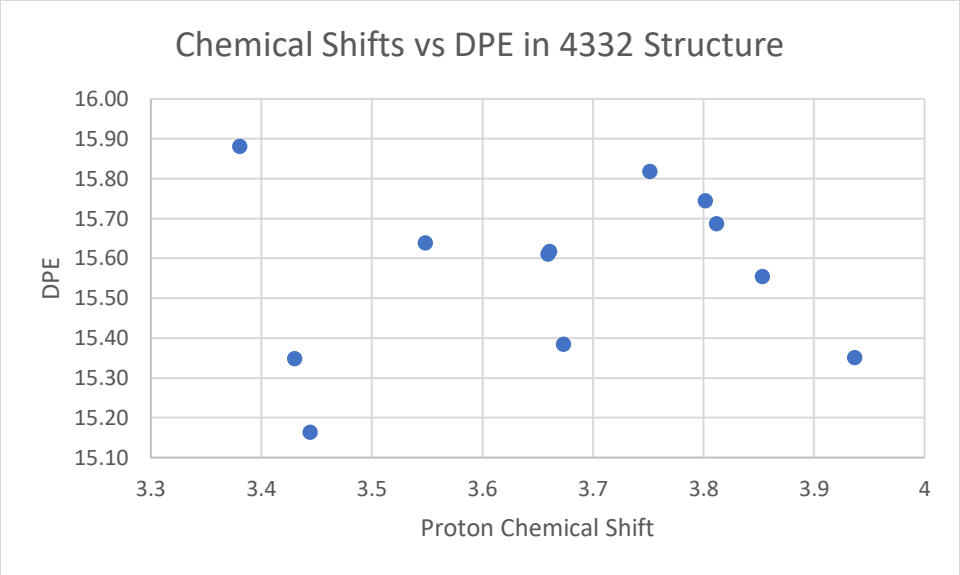

Figure 12. Deprotonation energy versus chemical shift in the 4332 structure in the absence of lanthanum species.

These shifts are comparable with findings from previous reports[110]. At the most stable position I, which is inside the sodalite bridge, the chemical shift of the protons in the system remains nearly unchanged. It is worth noting that at the second most stable position, the proton chemical shift for the hydrogen coordinated with La is 6.84 ppm which is a greater downfield shift than a Bronsted acid site proton. This is true of not only site I', but of all LaOH containing species. We observe that the chemical shift for all hydrogen directly connected to La has a chemical shift between 6.2 and 7.7 ppm. This downfield shift can be explained by assigning it to lanthanum's localized positive charge, which de-shields the proton electron cloud.

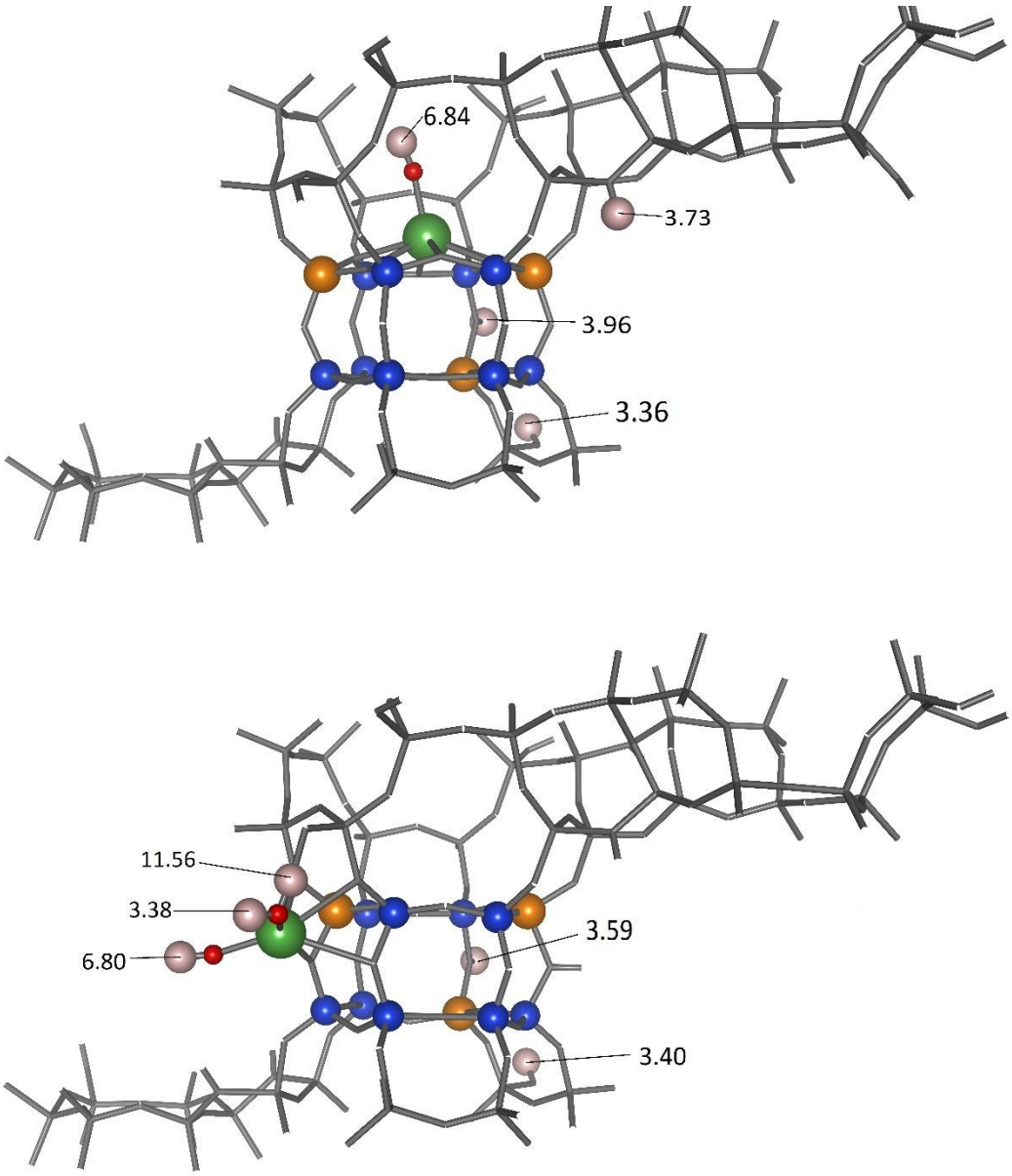

Figure 13. LaOH at site I' and $La(OH)_2$ at site III with some proton chemical shifts labeled. Chemical shifts are given in ppm. In the second figure, the proton with a chemical shift of 11.56 ppm is connected to an Al site and is coordinating with $La(OH)_2$. See Table 3 for more proton chemical shifts.

Table 3. Proton chemical shifts for the structures exchanged with lanthanum. Shaded values are protons connected with the La cation.

Proton Chemical Shifts (ppm)							
	I	I'	II	II'	II''	III	U
H#	La	LaOH	La(OH)2	LaOH	LaOH	La(OH)2	LaOH
1	3.71	6.84	4.66	7.10	6.26	6.80	7.59
2	3.73	3.73	5.39	3.87	3.94	3.38	3.93
3	3.57	3.77	3.81	3.68	3.69	3.77	3.72
4	3.60	3.36	3.74	3.39	3.36	3.60	3.30
5	3.68	3.61	3.41	3.74	3.74	3.40	3.70
6	3.54	3.68	3.63	3.78	3.76	3.63	3.51
7	3.85	3.55	3.74	3.53	3.54	11.56	4.28
8	3.59	3.84	3.61	3.91	3.86	3.38	3.86
9	3.46	3.60	4.00	4.11	4.14	3.85	4.19
10		3.96	3.52	3.74	3.75	3.44	3.65
11		3.36	3.56	4.09	3.90	3.59	3.83
12			3.76			3.78	
13			3.31			3.33	

The chemical shifts of Si are shown in Figures 14 through 16 for all of the single La arrangements shown in Table 3.

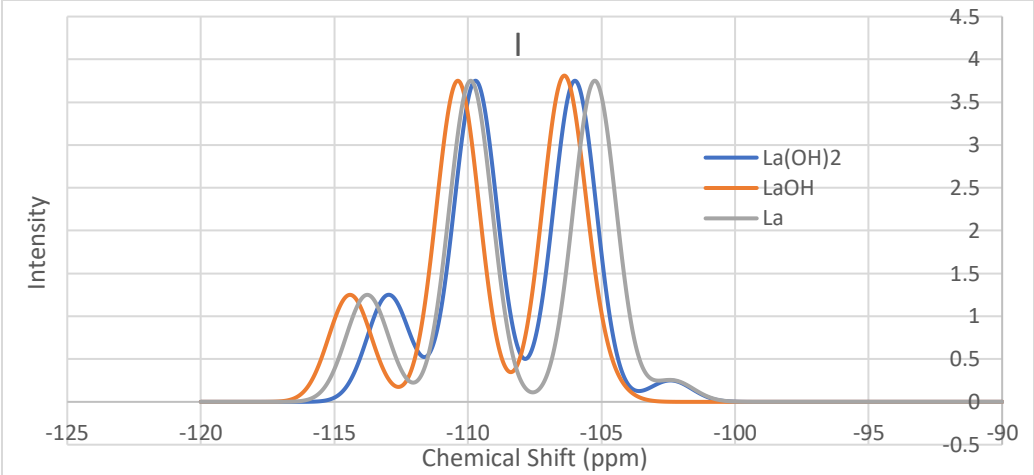

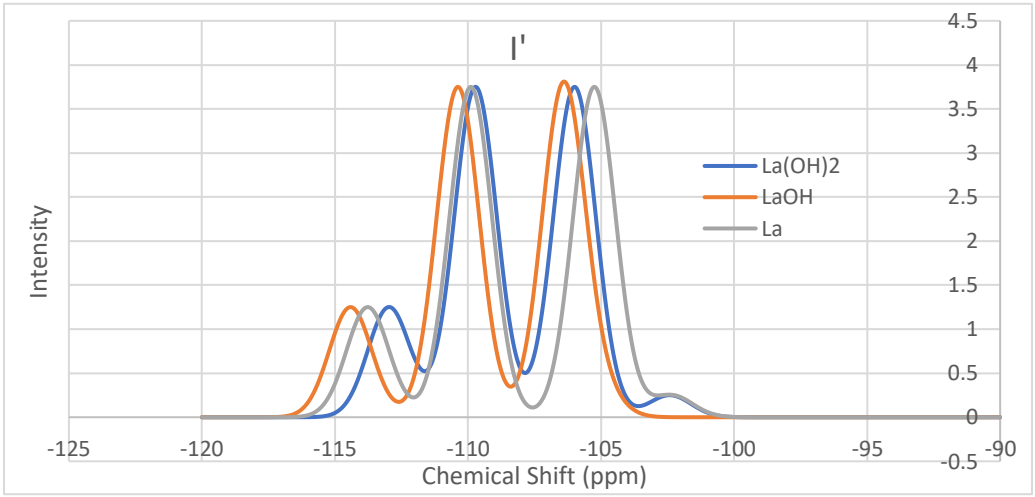

Figure 14. Si NMR spectra for sites I and I'. Si shifts are referenced to tetramethyl Silane.

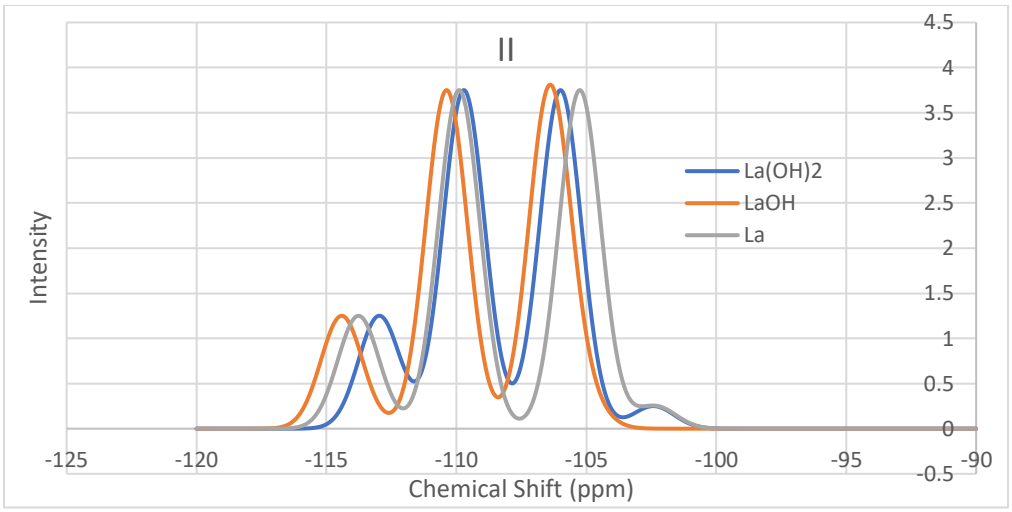

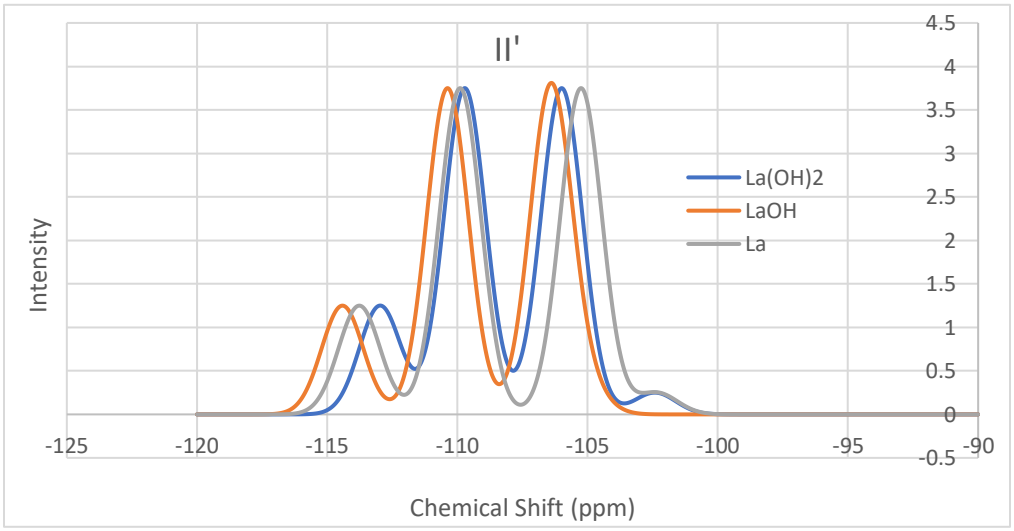

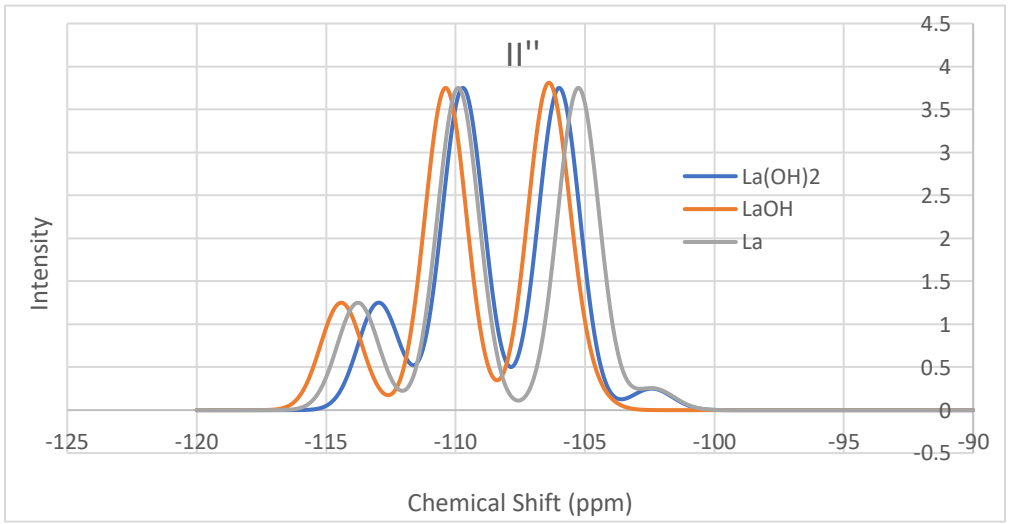

Figure 15. Si NMR spectra for sites II, II', and II''. Si shifts are referenced to tetramethyl Silane.

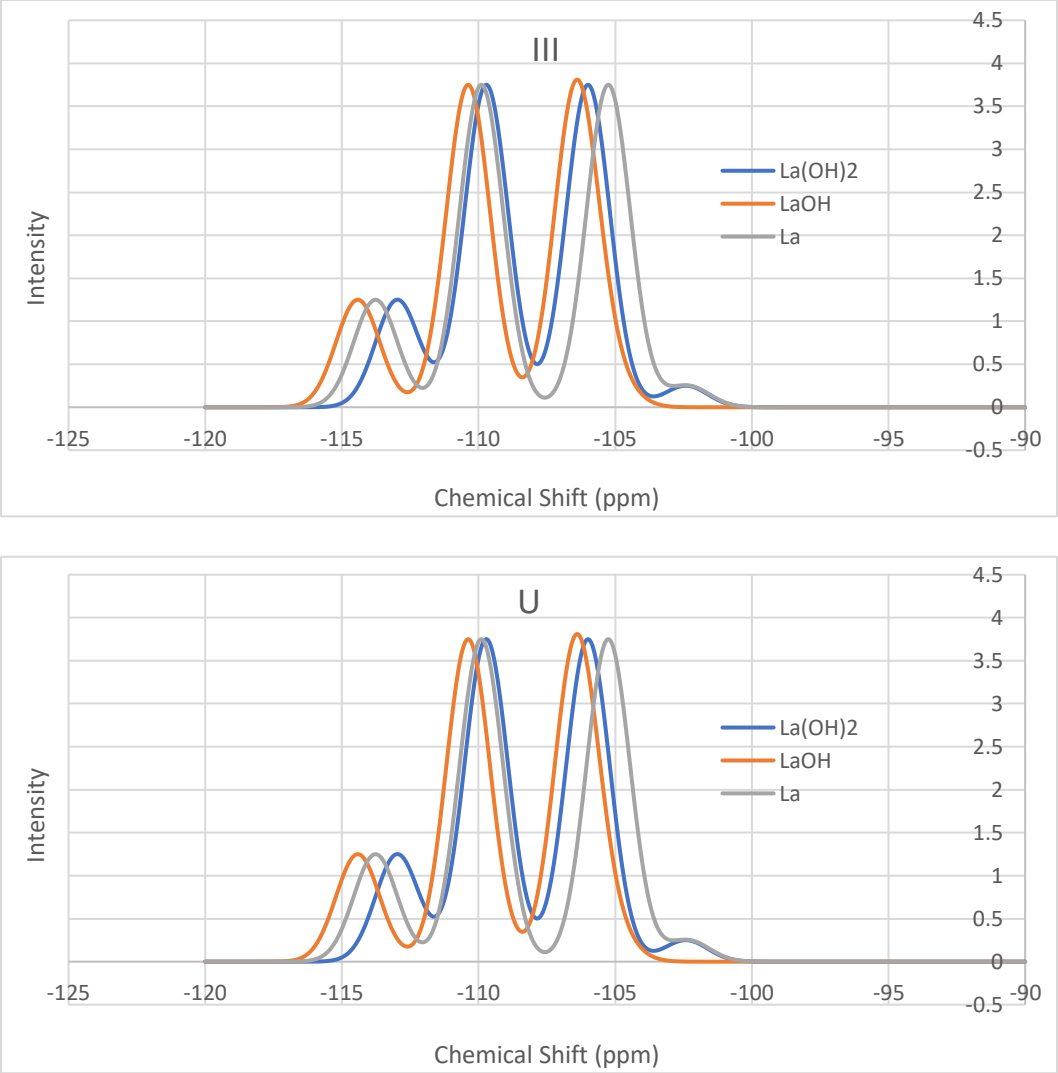

Figure 16. Si NMR spectra for sites III and U. Si shifts are referenced to tetramethyl Silane.

The Si NMR spectra shifted to the right for all La containing structures. Si attached to Al groups that participate in balancing the La charge shift to more negative, lower, values while other Si near the La cation shift towards more positive, higher, values. While LaOH always has the smallest shift to the right, the peaks for La and LaOH become similar for the peak associated with two Al neighbors. To the right of that peak La has the greater change in chemical shift and to the left $La(OH)_2$ has the greater shift. This means that Si-Al interactions

with a lower Al neighbor count are more affected by the presence of $La(OH)_2$ and silicon sites with more Al neighbors are effected to a greater degree by bare La^{3+} cations. This can be attributed to La^{3+} cations not interacting as much with sites near only one or two Al but tended to interact more with three Al connected with Si. Whereas, the $La(OH)_2$ has interactions with Si even if there is not an adjacent Al due to the hydroxide groups increasing its overall size. One dissenting publication from 2009, using Si MAS NMR, found that upon steam treatment of LaY structures at 800 degrees Celsius, the peaks for zero Al neighbors increases significantly and the peaks for two and three Al neighbors decrease. The effect is even greater for higher La loadings[109]. This appears to be in direct disagreement with the knowledge that La provides increased stability. The reason they see this result is due to the use of Si MAS NMR on zeolite Y. In this study, we found that a silicon next to one Al site, Si(1Al), will have a comparable Si chemical shift to silicon with no Al neighbors, Si(0Al). This occurs when the aluminum is balancing a charge from a La species. The reason they see more dealumination is because higher La loading causes Si chemical shifts to move towards lower values, thus appearing as if Al neighbors have been reduced. To further observe the effect of La on Si chemical shifts plots were generated comparing distance from La to Si and from Al to Si (see Figure 17 and Figure 18).

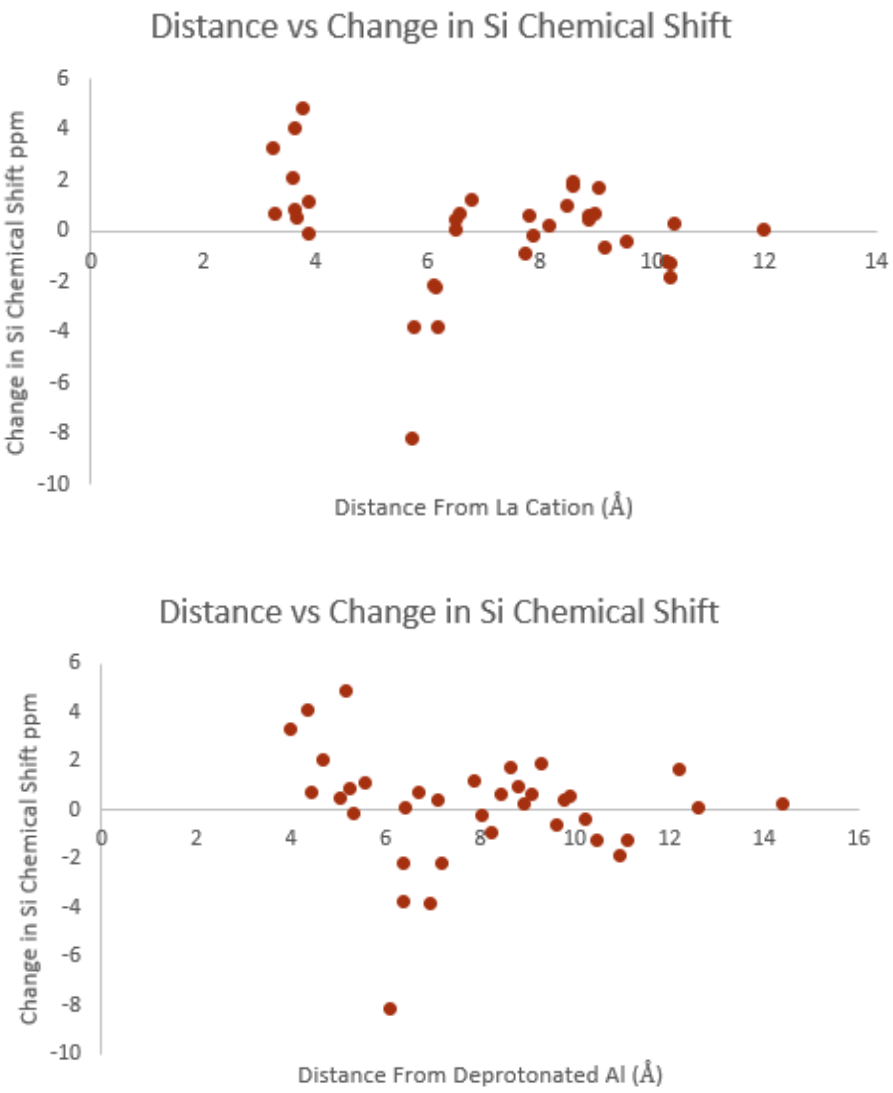

Figure 17. a) The x-axis is the distance from the lanthanum cation at site I (La^{3+}) measured in Angstrom. The y-axis is the difference in the Si-chemical shift betqeen the 4332 structure in the absence of La and the 4332 structure with La^{3+} at the I position (located in the center of the hexagonal prism). b) The x-axis for the second graph is the distance of Si atoms from the Al sites balancing the charge caused by La. There are three Al sites for this structure, this distance is calculated by averaging the distance of Si from all of these Al.

Figure 17.a reveals that the position of the La cation is not directly responsible for the change in Si-chemical shift, while Figure 17.b shows a potential trend where

the shift is less affected the further away it is from Al atoms that are balancing the charge caused by La. The trend is more clear in the case of $La(OH)_2$ at site III (as shown in Figure 18), located inside the supercage, since there is only one Al atom required to balance the charge thus allowing for a less complex system.

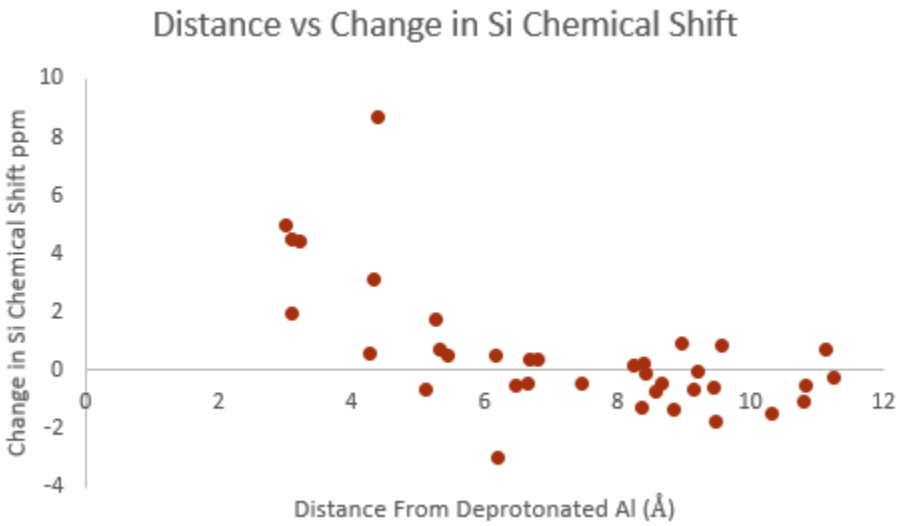

Figure 18. The x-axis is the distance of Si atoms from the charge balancing Al. The y-axis is the difference in chemical shift between the 4332 structure before La and the 4332 structure containing $La(OH)_2$ at the III position, located inside the supercage.

A higher downfield proton chemical shift does not necessarily mean that a given proton is more acidic. DPE (deprotonation energy) is a more intrinsic measure of acidity. The DPE values were calculated for hydrogen atoms connected to La for the most stable structures at each position within the unit cell. As can be seen in Figure 19, the chemical shift and deprotonation energy are generally higher for protons connected to lanthanum molecules. There was not any noticeable difference in DPE/Chemical shift between clusters with two or three La and thus they were included in the same category.

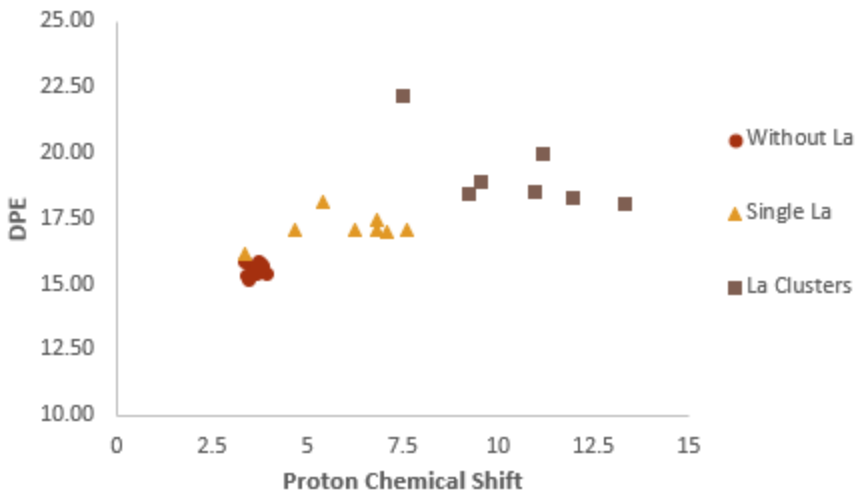

Figure 19. Chemical shift (ppm) plotted against DPE (eV). The red circles are for the 12 protons contained in the 4332 unit cell without La. The yellow triangles are the protons contained in the OH^- groups bonded with La, only the structures in Figure 3 are considered. The squares are the hydrogens attached to lanthanum groups held within the sodalite for both two and three La.

There was no direct correlation between DPE and proton chemical shifts found for this system. This means that the acid strength of protons in the framework is not only the result of electronic shielding caused by the presence of Al and La species but is dependent on another unknown factor, such as the effective charge on the protons. In order to determine this, further calculations must be performed, for charge analysis and for specific reactions to visualize the effect of La cations on the reaction pathways.

Chapter 4: Conclusions and Future Work

This study has found that the 3333 arrangement of Al sites is the most stable. Despite this, the 4332 structure is the arrangement that occurs in practice as seen through comparison of NMR peaks. Position I, located in the center of the hexagonal prism, was found to be the most stable lanthanum position for La-exchanged zeolite Y. Lanthanum clusters of three have reduced stability compared to lanthanum cations scattered to the more stable positions. However, clusters of two lanthanum cations contained in the sodalite are preferred over all other orientations. Si-chemical shifts move to higher values with the addition of La. A trend was found correlating the distance of Si from charge balancing Al sites to Si-chemical shift. Figure 12 shows that no direct correlation exists between the DPE and proton chemical shift. The location of lanthanum and number of bonded OH groups are likely similar for cerium exchanged zeolite Y since they have a similar stabilizing effect and negative charge[48]. Clusters of four or more La will likely be less stable than two lanthanum since it is at a minimum (stability increases from one to two and then decreases upon addition of the third La).

Further characterization of the LaY structure would provide more insight into stabilizing effects as well as acid site density. It would be of interest to elucidate the location and nature of EFAL species and how they interact with La. We do not know whether the EFAL sites will draw La species to them, nor do we know how active these La species would be if they were coordinated with extra framework aluminum. Another point requiring clarification is in regards to the

acid strength of lanthanum OH groups. From the DPE results these groups are shown to be weak Bronsted acid sites, however, these species may have the capacity to act as strong Lewis acid sites. Though no trend was found between DPE and proton chemical shift, a trend is expected to be found between the Bader and the proton chemical shift, since the Bader charge is a measure of the electron cloud and chemical shift measures the electron field. Further experimentation needs to be performed in order to better understand the process by which catalytic activity is increased, DFT simulations of specific reactions can be prepared using the lanthanum positions and zeolite structure described here as a model.

References

1. Vogt, E. T. C., Weckhuysen, B. M, Fluid Catalytic Cracking: Recent Developments on the Grand Old Lady of Zeolite Catalysis. *Chem. Soc. Rev.* **2015**.
2. Eser, D. S., Fluid Catalytic Cracking (FCC). *Penn State College of Earth and Mineral Sciences* **2021**.
3. G., S. J., The Chemistry and Technology of Petroleum 3rd Ed. *New York: CRC Press* **1999**.
4. Company, S., The Houdry Process – A National Historic Landmark. *American Chemical Society* **1996**.
5. Breck, D. W., Crystalline Zeolite Y. *US3,130,007A* **1964**.
6. Tezel, D. F. H., (Energy - Storage, Membranes, Adsorption Research and Technology). **2021**.
7. Christian Baerlocher, L. B. M., David H. Olson, Atlas of Zeolite Framework Types (Sixth Edition). *Elsevier* **2007**.
8. W. Vermeiren, J. P. G., Impact of Zeolites on the Petroleum and Petrochemical Industry. *Topics in Catalysis* **2009,** *52*.
9. Ribeiro, F. R., Use of Platinum HY Zeolite and Platinum H Mordenite in the Hydroisomerization of N-Hexane. *Zeolites: Science and Technology* **1984**.
10. Jaap N. Louwen, S. S., Katarina Stanciakova, Rosa E. Bulo, Bert M. Weckhuysen, Eelco T. C. Vogt, Role of Rare Earth Ions in the Prevention of Dealumination of Zeolite Y for Fluid Cracking Catalysts. *ACS Publications* **2020**.
11. Thomas F. Degnan, J., Applications of zeolites in petroleum refining. *ExxonMobil Corporation, Corporate Strategic Research* **2000**.
12. Li, C.-Y., Rees, L. V. C. , The Thermal Stability of Faujasites with Different Si/AI Ratios. Zeolites. **1986,** *6* (1), 5.
13. R. Carvajal, P. C., J.H. Lunsford, The role of polyvalent cations in developing strong acidity: A study of lanthanum-exchanged zeolites(Article). *Journal of Catalysis* **1990**.
14. Lemos F., R. R. F., Kern M., Giannetto G., Guisnet M., Influence of lanthanum content of LaHY catalysts on their physico-chemical and catalytic properties. Comparison with CeHY catalysts. *Applied Catalysis* **1988**.
15. Lemos F., R. F. R., Kern M., Giannetto G., Guisnet M., Influence of the cerium content of CeHY catalysts on their physicochemical and catalytic properties. *Applied Catalysis* **1987**.
16. J.W. Roelofsen, H. M., R.L. de Groot, P.C.M. van Woerkom, H. Angad Gaur, Effect of Rare Earth Loading in Y-Zeolite on its Dealumination during Thermal Treatment. *Studies in Surface Science and Catalysis* **1986,** *28*, 8.
17. Eduardo Falabella Sousa-Aguiar ab Vera, L. D. C. a., Fatima Maria Zanon Zotin c, Ronaldo Luiz Correa dos Santos c, A Fourier transform infrared spectroscopy study of La-, Nd-, Sm-, Gd- and Dy-containing Y zeolites. *Microporous and Mesoporous Materials* **1998**.
18. Edward F.T. Lee, L. V. C. R., Effect of calcination on location and valency of lanthanum ions in zeolite Y. *Zeolites* **1986,** *7* (2), 5.

19. Horst Winkler, K.-H. S., On the position of rare earth cations in zeolite Y. *Zeolites* **1989,** *9* (5).
20. Klinowski, J., Ramdas, S. Thomas, J. M. Fyfe, C. A. Hartman, J. S. , A Re-Examination of Si, Al Ordering in Zeolites NaX and NaY. *J. Chem. Soc* **1982**.
21. Sch€ußler, F. P., A. Evgeny,. Kolvenbach, Robin,. Sievers, Carsten,. § Hensen, J. M. Emiel,. Santen, A. van Rutger,. and Lercher A. Johannes, Nature and Location of Cationic Lanthanum Species in High Alumina Containing Faujasite Type Zeolites. *The Journal of Physical Chemistry* **2011**.
22. Julius Scherzer, J. L. B., Fred D. Hunter, Structural Characterization of Hydrothermally Treated Lanthanum Y

Zeolites. I. Framework Vibrational Spectra and Crystal Structure. *W. R. Grace & Co., Washington Research Center* **1974**.
23. Jong R. Sohn, S. J. D., Jack H. Lunsford, Daniel J. O'Donnell Determination of framework aluminium content in dealuminated Y-type zeolites: a comparison based on unit cell size and wavenumber of i.r. bands. *Zeolites* **1985,** *6* (3).
24. I. R. Subbotina, V. B. K., IR Spectroscopic Study of Cyclopropane Adsorption on Zeolite Y: I. Cyclopropane Adsorption and Transformation on Sodium- and Hydrogen-Exchanged Zeolite Y. *Kinetics and Catalysis* **2002,** *43*.
25. M. Jia, H. L., and H. F6rster I.r. studies on the acidity of dealuminated Y

zeolite with different probe molecules *Zeolites* **1992,** *12* (1).
26. LibreTexts, Infrared Spectroscopy. In *Chemistry*, 2020.
27. Ross, J. R. H., *Contemporary Catalysis Fundamentals and Current Applications*. Elsevier: 2019.
28. E. M. Flanigen , H. K., H. A. Szymanski Molecular Sieve Zeolites-I. **1971,** *Adv. Chem. Ser.*
29. J. W. Roelofsen, H. M., R. L. de Groot, P. C. M. van Woerkom, H. Angad Gaur, Effect of Rare Earth Loading in Y-Zeolite on its Dealumination during Thermal Treatment. *Studies in Surface Science and Catalysis* **1986,** *28*.
30. S. Jolly, J. S. a. J. C. L., FT-IR study of hydrocarbon conversion on dealuminated HY

zeolites in working conditions *Journul of Mokculur Catalysis* **1994**.
31. J. Scherzer, J. L. B., Ion exchanged ultrastable Y zeolites: I. Formation and structural characterization of lanthanum-hydrogen exchanged zeolites. *Journal of Catalysis* **1977**.
32. Xionghou Gao, Zhengxing Qin, Baojie Wang, Xiaozheng Zhao, Jiangcheng Li, Hongjuan Zhao,; Honghai Liu, B. S., High silica REHY zeolite with low rare earth loading as high-performance catalyst for heavy oil conversion. *Applied Catalysis A: General* **2012**.
33. Vartak, A. HEXANE CRACKING ON Y ZEOLITES: ACTIVITY ENHANCEMENT AND ITS

POSSIBLE REASONS. University of Oklahoma, 2016.
34. Jun Huang, Y. J., V. R. Reddy Marthala, Yean Sang Ooi, Michael Hunger, Regioselective H/D Exchange at the Side-Chain of Ethylbenzene on

Dealuminated Zeolite H-Y Studied by In Situ MAS NMR–UV/Vis Spectroscopy. *Communication* **2008**.
35. Mariusz Gackowski, K. T., Łukasz Kuterasiński, Jerzy Podobiński, Bogdan Sulikowski, Jerzy Datka, Spectroscopic IR and NMR studies of hierarchical zeolites obtained by desilication of zeolite Y: Optimization of the desilication route. *Microporous and Mesoporous Materials* **2019,** *281*.
36. Shanqing Yu, J. Y., Wei Lin, Jun Long, Shang-Bin Liu Effects of Lanthanum Incorporation on Stability, Acidity and Catalytic Performance of Y Zeolites. *Catalysis Letters* **2020,** *151*.
37. I. I. Rabi, J. R. Z., S. Millman, P. Kusch, A New Method of Measuring Nuclear Magnetic Moment. *Phys Rev* **1938,** *53*.
38. Dr. Dietmar Kennepohl, P. S. F., Dr. Richard Spinney, Chemical Shifts and Shielding. *Chemistry LibreTexts* **2020**.
39. Cory, P. D., A Hands-On Introduction to Nuclear Magnetic Resonance. *MIT OpenCourseWare, Massachusetts Institute of Technology* **1997**.
40. Calgary, U. o. Nuclear Magnetic Resonance (NMR) Spectroscopy.
41. University, M. S. Basic Practical NMR Concepts:

A Guide for the Modern Laboratory.
42. Wenzel, T., Classical Description of NMR Spectroscopy. **2020**.
43. LibreTexts, C., 13.S: Structure Determination - Nuclear Magnetic Resonance Spectroscopy (Summary). **2020**.
44. Clark, J., Interpreting C-13 NMR Spectra. **2020**.
45. Abdul-Hamid, M. E., The Strengths and Weaknesses of NMR Spectroscopy and Mass Spectrometry with Particular Focus on Metabolomics Research. *Metabonomics* **2015**, 33.
46. Jenkins, T. M. A. a. J. E., HR-MAS NMR Spectroscopy in Material Science. *Advanced Aspects of Spectroscopy* **2012**.
47. University, E., Introduction to Solid State NMR. **2021**.
48. Bejoy Thomas, B. B. D., S. Sugunan, Rare earth exchanged (Ce3+, La3+ and RE3+) H–Y zeolites as solid acid catalysts for the synthesis of linear alkyl benzenes. *Microporous and Mesoporous Materials* **2006**.
49. R. Beaumont, D. B., X, Y, Aluminum-Deficient and Ultrastable Faujasite-Type Zeolites

I. Acidic and Structural Properties. *Journal of Catalysis* **1971**.
50. Na Wang, M. Z., Yingzhe Yu, Distribution of aluminum and its influence on the acid strength of Y zeolite. *Microporous and Mesoporous Materials* **2013**.
51. P. S. Niphadkar, K. R. P., P. N. Joshi, Characterization of surface acid sites in tin-silicalite-1 (Sn-MFI) molecular sieve by X-ray photoelectron spectroscopy. *Microporous and Mesoporous Materials* **2011**.
52. B. Dragoi, E. D., C. Guimon, A. Auroux, Acidic and adsorptive properties of SBA-15 modified by aluminum incorporation. *Microporous and Mesoporous Materials* **2009**.
53. Andrew J. Jones, R. T. C., Stacey I. Zones, Enrique Iglesia, Acid strength and solvation in catalysis by MFI zeolites and effects of the identity, concentration and location of framework heteroatoms. *Journal of Catalysis* **2014**.

54. H. V. Brand, L. A. C., L. E. Iton, Ab initio molecular orbital cluster studies of the zeolite ZSM-5. 1. Proton affinities. *J. Phys. Chem* **1993**.
55. H. V. Brand, L. A. C., L. E. Iton, Computational studies of acid sites in ZSM 5: dependence on cluster size. *J. Phys. Chem* **1992**.
56. Aleksei Vjunov, M. W., Niranjan Govind, Thomas Huthwelker, Hui Shi,; Donghai Mei, J. L. F., Johannes A. Lercher, Tracking the Chemical Transformations at the Brønsted Acid Site

upon Water-Induced Deprotonation in a Zeolite Pore. *Chemistry of Materials* **2017**.
57. A. Chatterjee , T. I., T. Ebina, A. Miyamoto, Density functional study for estimating Brsnsted acid site strength.

in isomorphously substituted ZSM-5 *Microporous and Mesoporous Materials* **1998**.
58. Dr. Stepan Sklenak, D. J. D., Dr. Chengbin Li, Dr. Blanka Wichterlová, Dr. Vendula Gábová, Dr. Marek Sierka, Professor Joachim Sauer, Aluminum Siting in Silicon-Rich Zeolite Frameworks: A Combined High-Resolution 27Al NMR Spectroscopy and Quantum Mechanics / Molecular Mechanics Study of ZSM-5. *Communication* **2007**.
59. van Bokhoven, J. A.; Roest, A. L.; Koningsberger, D. C.; Miller, J. T.; Nachtegaal, G. H.; Kentgens, A. P. M., Changes in Structural and Electronic Properties of the Zeolite Framework Induced by Extraframework Al and La in H-USY and La(x)NaY: A 29Si and 27Al MAS NMR and 27Al MQ MAS NMR Study. *The Journal of Physical Chemistry B* **2000,** *104* (29), 6743-6754.
60. Jırı Dedecek, S. S., Chengbin Li, Blanka Wichterlova, Vendula Gabova,; Jırı Brus, M. S., Joachim Sauer, Effect of Al-Si-Al and Al-Si-Si-Al Pairs in the ZSM-5 Zeolite Framework on the 27Al

NMR Spectra. A Combined High-Resolution 27Al NMR and DFT/MM Study. *Journal of Physical Chemistry* **2009**.
61. Jones, R. O., Density functional theory: Its origins, rise to prominence, and future. *Rev. Mod. Phys* **2015**.
62. Micromeritics, A Brief History of Density Functional Theory Applied to Extracting Information from the Physical Adsorption Isotherm.
63. W. Kohn, L. J. S., Self-Consistent Equations Including Exchange and Correlation Effects. *Physical Review* **1965**.
64. E, S., Quantisation as an eigen value problem. *Annalen Der Physik* **1926**.
65. E, S., An undulatory theory of the mechanics of atoms and molecules. *Phys Rev* **1926**.
66. PAM, D., The quantum theory of the electron. *Proc R soc Lond Ser A Contain Pap Math Phys Character* **1928**.
67. PAM, D., The quantum theory of the electron—part II. *Proc R soc Lond Ser A Contain Pap Math Phys Character* **1928**.
68. PAM, D., On the quantum theory of electrons. *Physikalische Zeitschrift* **1928**.

69. Robin Haunschild, A. B., Bernie French A comprehensive analysis of the history of DFT based on the bibliometric method RPYS. *Journal of Cheminformatics* **2019,** *11*.
70. Yaresko, A., Density Functional Theory for beginners. *Institute for Metal Physics* **2017**.
71. Fermi, E., Eine statistische Methode zur Bestimmung einiger Eigenschaften des Atoms und ihre Anwendung auf die Theorie des periodischen Systems der Elemente. *Zeitschrift für Physik* **1928,** *48*.
72. Thomas, L. H., The calculation of atomic fields. *Mathematical Proceedings of the Cambridge Philosophical Society* **1927,** *23* (5).
73. Douglas Rayner Hartree, W. H., Self-consistent field, with exchange, for beryllium. *Proc. R. Soc. Lond. A* **1935**.
74. Fock, V., Näherungsmethode zur Lösung des quantenmechanischen Mehrkörperproblems. *Zeitschrift für Physik* **1930,** *61*.
75. Slater, J. C., A Simplification of the Hartree-Fock Method. *Phys. Rev* **1951**.
76. S. H. Vosko, L. W., M. Nusair, Accurate spin-dependent electron liquid correlation energies for local spin density calculations: a critical analysis. *Canadian Journal of Physics* **1980,** *48* (8).
77. John P. Perdew, K. B., Matthias Ernzerhof, Generalized Gradient Approximation Made Simple. *Phys. Rev. Lett.* **1996,** *77*.
78. Wang, J. P. P. a. Y., Accurate and simple analytic representation of the electron-gas correlation energy. *Phys. Rev. B* **1992,** *45*.
79. Jianmin Tao, J. P. P., Viktor N. Staroverov, Gustavo E. Scuseria, Climbing the Density Functional Ladder: Nonempirical Meta–Generalized Gradient Approximation Designed for Molecules and Solids. *Phys. Rev. Lett.* **2003,** *91*.
80. John P. Perdew, S. K., Aleš Zupan, Peter Blaha, Accurate Density Functional with Correct Formal Properties: A Step Beyond the Generalized Gradient Approximation. *Phys. Rev. Lett.* **1999,** *82*.
81. Yan Zhao, D. G. T., A new local density functional for main-group thermochemistry, transition metal bonding, thermochemical kinetics, and noncovalent interactions. *J. Chem. Phys* **2006**.
82. Carlo Adamo, V. B., Toward reliable density functional methods without adjustable parameters: The PBE0 model. *J. Chem. Phys.* **1999**.
83. Yan Zhao, N. E. S., D. G. Truhlar, Exchange-correlation functional with broad accuracy for metallic and nonmetallic compounds, kinetics, and noncovalent interactions. *J. Chem. Phys.* **2005**.
84. Becke, A. D., A new mixing of Hartree–Fock and local density‐functional theories. *J. Chem. Phys* **1993**.
85. John P. Perdew, M. E., Rationale for mixing exact exchange with density functional approximations. *J. Chem. Phys* **1996**.
86. Jochen Heyd, G. E. S., Erratum: "Hybrid functionals based on a screened Coulomb potential" [J. Chem. Phys. 118, 8207 (2003)]. *J. Chem. Phys* **2006**.
87. VASP The Vienna Ab initio Simulation Package: atomic scale materials modelling from first principles.

88. Mohamed Hacene, A. A.-S., Xavier Rozanska, Diego Klahr, Thomas Guignon, Paul Fleurat-Lessard, Accelerating VASP electronic structure calculations using graphic processing units. *Journal of Computational Chemistry* **2012**.
89. Mohamed Abatal, A. R. R.-S., Norge Cruz Hernández, A DFT-based simulated annealing method for the optimization of global energy in zeolite framework systems: Application to natrolite, chabazite and clinoptilolite. *Microporous and Mesoporous Materials* **2020**.
90. Hafner, J., Ab‐Initio Simulations of Materials Using VASP: Density‐Functional Theory and Beyond. *Journal of Computational Chemistry* **2008,** *29*, 2044–2078.
91. I. Georgieva, N. T., N. Dodoff, D. Kovacheva, DFT study of the molecular and crystal structure and vibrational analysis of cisplatin. *Elsevier* **2017**.
92. Özgen Yalçın, I. Ö., DFT investigation of high temperature water gas shift reaction on chromium–iron mixed oxide catalyst. *International Journal of Hydrogen Energy* **2014,** *39* (34).
93. Sharankumar Shetty, S. S., Suman Kumar Jana, G. Sreenivasarao, Investigation of CHx (x = 2–4) Adsorption on Mo2C and Mo4C2 Sites Incorporated in ZSM-5 Zeolite Using Periodic-DFT Approach. *Catalysis Letters* **2017,** *148*.
94. Kresse G., F. J., Efficient iterative schemes for ab initio total-energy calculations using a plane-wave basis set. *Phys Rev B* **1996,** *54*.
95. Hoffman, A.; DeLuca, M.; Hibbitts, D., Restructuring of MFI Framework Zeolite Models and Their Associated Artifacts in Density Functional Theory Calculations. *The Journal of Physical Chemistry C* **2019,** *123* (11), 6572-6585.
96. Matt Spurlock, S. H. Evaluating the Source of Silicon in Oil.
97. Walter Loewenstein, M. L., The Distrubution of Aluminum in the Tetrahdra of Silicates and Aluminates. *Am. Mineral* **1954,** *39*.
98. Fletcher, R. E., Ling, S., Slater, B. , Violations of Löwenstein's Rule in Zeolites. *Chem. Sci* **2017**.
99. Fischer, D. M., Proton Acidity and Proton Mobility in ECR-40, a Silicoaluminophosphate that Violates Löwenstein's Rule. *Chemistry Europe* **2019**.
100. Xiaomin Tang, Z. L., Ling Huang, Wei Chen, Chengbin Li, Guiru Wang, Guangchao Li, Xianfeng Yi, Anmin Zheng, Violation or Abidance of Löwenstein's Rule in Zeolites Under Synthesis Conditions? *ACS Catalysis* **2019**.
101. Yates J. R., P. C. J., Mauri F. , Calculation of NMR chemical shifts for extended systems using ultrasoft pseudopotentials. *Phys Rev B* **2007,** *76*.
102. Pickard C. J., M. F., All-electron magnetic response with pseudopotentials: NMR chemical shifts. *Phys Rev B* **2001,** *63*.
103. Cambridge, U. o., Linear Response. **2019**.
104. Melchior, M. T., Vaughan, D. E. W. Pictroski, C. F. , Local Environment Fine Structure in the 29Si NMR Spectra of Faujasite Zeolites. *J. Phys. Chem. C* **1995**.
105. Zeets M., R. D. E., Wang B. , Enhanced chemical activity and wettability at adjacent Bronsted acid sites in HZSM-5. *Catalysis Today* **2018,** *312*, 7.

106. Robson, H., Verified Synthesis of Zeolitic Materials: Second Edition. *Elsevier* **2001**.
107. Zhengxing Qin, B. S., Xionghou Gao, Feng Lin, Baojie Wang, Chunming Xu, Mesoporous Y zeolite with homogeneous aluminum distribution obtained by sequential desilication–dealumination and its performance in the catalytic cracking of cumene and 1,3,5-triisopropylbenzene. *Journal of Catalysis* **2011**.
108. S. Huber, H. K., Adsorption of CO on sodium containing X- and Y-zeolites and determination of the aluminum distribution. *Elsevier* **1999,** *181* (2).
109. Pablo García, E. L., Julia Aguilar, Víctor Lara Fractal Extra-Framework Species in De-aluminated LaY Zeolites and Their Catalytic Activity. *Catalysis Letters* **2009,** *128*.
110. Michael Hunger, D. F., Harry Pfeifer, Dagmar Prager, Wladimir Reschetilowski, Proton MAS NMR studies of hydroxyl groups in alkaline earth cation-exchanged zeolite Y. *Chemical Physics Letters* **1989,** *163* (2-3), 4.

Appendix A: Details of the INCAR Files

A.1: Stability Calculations

PREC = NORMAL

EDIFF = 1e-6

GGA = PE

LREAL = Auto

ALGO = FAST

ENCUT= 500

NSW = 500

NELM = 40

IBRION = 2

EDIFFG = -0.02

POTIM = 0.5

ISIF = 3

ISMEAR = 0

SIGMA = 0.2

IVDW = 11

A.2: Chemical Shift Calculations

PREC = A

EDIFF = 1e-8

GGA = PE

LREAL = Auto

ALGO = FAST

ENCUT = 600

NSW = 0

NELM = 40

IBRION = 2

EDIFFG = -0.02

POTIM = 0.5

ISMEAR = 0

SIGMA = 0.1

IVDW = 11

LCHIMAG = .TRUE.

DQ = 0.001

ICHIBARE = 1

LNMR_SYM_RED = .TRUE.

NSLPLINE = .TRUE.

Appendix B: Raw Data

Table B1. Number of Si with 0, 1, 2, 3, or 4 Al neighbors for structures 6600, 4332, and 3333 compared to results from Klinowski's research.

Al Neighbors	0	1	2	3	4
6600	16	8	0	8	4
4332	5	15	15	1	0
3333	8	10	16	2	0
Klinowski A[20]	4	16	16	0	0

Table B2. Energetics of each Al orientation accompanied by the optimized unit cell size.

Distribution of 12 Al	Relative Energy (eV)	Relative Energy (kcal/mol)	Unit Cell Size
Zeolite Y 6600	1.4574	33.5202	23.8173
Zeolite Y 3333	0	0	24.8336
Zeolite Y 4332	0.2391	5.4993	24.8356

Table B3. Energetics of each site with each hydroxide coordination. N/A is for sites that, when the energy was optimized, migrated to another site as a result of instability.

Sites	LaOH2	LaOH	La
I	-2.32	-2.79	-3.36
I'	-3.18	-3.22	-1.96
II	-1.58	N/A	N/A
II'	-2.23	-2.42	-1.73
II''	-2.02	-2.95	-1.93
III	-2.86	-2.28	-0.58
U	-1.83	-2.04	-0.88